12-2016

Photoluminescence Studies of Amorphous Boron Carbide and Tungsten Diselenide Thin Films

David M. Allendorfer
University of Nebraska - Lincoln, david_allendorfer@yahoo.com

Photoluminescence Studies of Amorphous Boron Carbide and Tungsten Diselenide Thin Films

by

David Allendorfer

A Thesis

Presented to the Faculty of

The Graduate College at the University of Nebraska

In Partial Fulfillment of Requirements

For the Degree of Master of Science

Major: Electrical Engineering

Under the Supervision of Professor Natale Ianno

Lincoln, Nebraska

December, 2016

Photoluminescence Studies of Amorphous Boron Carbide and Tungsten Diselenide Thin Films

David Allendorfer, M. S.

University of Nebraska, 2016

Adviser: Natale J. Ianno

For many years scientists and engineers have been researching semi-conducting materials for use in a broad array of electronic devices. With the growing demand for faster, smaller and more efficient electronics, new materials must be characterized and their properties quantified. The focus of this thesis is to develop a system to measure photoluminescence in opto-electronic materials. Photoluminescence measurements are important because it can give researchers valuable information about a material's band structure. This thesis begins by presenting the carrier recombination mechanisms and how they apply to photoluminescence. A system was developed to measure photoluminescence spectroscopy. This system was tested with various known materials then used to characterize new materials.

Acknowledgements

I'd like to take this time and thank all of the people who helped me in my research. I first want to thank my adviser Dr. Natale Ianno who has been a great teacher and understanding boss these several years. I'm grateful for the guidance I've received from him. I'd like to thank Dr. Craig Zuhlke for all of his help with the laser setup and for putting up with my incessant questions. His help has been invaluable to me in my research. I also want to thank Dr. Dennis Alexander and Dr. Ming Han for sitting on my graduate committee. Lastly I want to thank my wife Courtney for supporting me through this stressful time. Whenever life sucked you were always there to make it better.

Table of Contents

List of Figures

List of Tables

Chapter 1

Introduction

For many years scientists and engineers have been researching semi-conducting materials for use in a broad array of electronic devices including diodes, transistors, lights, sensors, solar cells and many more[1-7]. With the growing demand for faster, smaller and more efficient electronics, scientists are always looking to newer and more exotic semi-conducting materials. These new unknown materials need to be characterized and their properties quantified.

In steady state photoluminescence measurements a continuous wave (CW) laser is incident onto a direct band gap semiconductor material such as GaAs [8-10]. The semiconductor absorbs the light generating excess electron-hole pairs. The electron-hole pairs then recombine and light is re-emitted in the form of a photon near the band gap energy. The intensity is then recorded as a function of the photoluminescent wavelength.

The focus of this thesis is to develop a system to measure photoluminescence in opto-electronic materials. Photoluminescence measurements are important for research and development of semiconductor materials because it can give researchers valuable information about a material's band structure. Photoluminescence is useful because it can give a quantitative look at the quality of a material. This is necessary for the process of developing and testing solid-state electronic devices.

Photoluminescence is limited to materials with a direct band gap [9], which is not an issue in this work since the two materials under study, a-B_5C:H and WSe_2 are direct gap materials.

1.1 Recombination Theory

Photoluminescence is heavily dependent on the recombination mechanisms of a material's minority carriers. The dominating recombination mechanism is very sensitive to impurities or defects.

The minority carrier lifetime is defined as the average time it takes an excess minority carrier to recombine. The minority carrier lifetime is a function of three different types of carrier recombination: radiative recombination, Shockley-Read-Hall recombination, and Auger recombination. [11]

$$\frac{1}{\tau_{bulk}} = \frac{1}{\tau_{SRH}} + \frac{1}{\tau_{rad}} + \frac{1}{\tau_{Auger}} \quad (1)$$

1.1.1 Radiative Recombination

Radiative (or band to band) recombination occurs in direct band gap semiconductors when an electron recombines directly with a hole. Radiative recombination is dependent on the density of electrons and holes. When radiative recombination occurs, a photon is emitted. The energy of the emitted photon is close to that of the band gap, depending on the effect phonon interaction plays in the

recombination mechanisms. The best example of radiative recombination is an LED. This is the dominant mechanism in direct band gap materials such as GaAs. In indirect band gap semiconductors such as silicon, the radiative lifetime (τ_{rad}) is very large. This is because the valence and conductions bands do not line up causing the direct band to band recombination to be far less frequent. [10] Because the radiative lifetime is very large it can usually be neglected.

The simple band to band recombination rate, R, is given by the following equation:

$$R = Bnp \ (2)$$

Where B is the radiative recombination coefficient specific to the semiconductor, and n and p are the total concentrations of electrons and holes respectively. In non-equilibrium circumstances such as carrier generation or recombination, $n=n_0+\Delta n$ and likewise $p=p_0+\Delta p$ where n_0 and p_0 are the respective equilibrium electron and hole concentrations while Δn and Δp are the transient electron and hole concentrations. [9] At equilibrium the recombination and generation rates are equal because the product of the electron and hole densities is constant ($n_0 * p_0 = n_i^2$), but in an excess of minority carriers the recombination rate increases to drive the system back into equilibrium. In a deficit of minority carriers, the generation rate increases to drive the system back into equilibrium. [14] In the presence of excess carriers the equation becomes:

$$R_{rad} = B(n_0 + \Delta n)(p_0 + \Delta p) \quad (3)$$

1.1.2 Shockley-Read-Hall Recombination

Shockley-Read-Hall (SRH) recombination, also referred to as trap-assisted recombination, occurs in semiconductor materials with defects in the crystalline structure. These structural defects can trap electrons or holes within the forbidden region of the band gap. These traps can be unintentional (imperfect material growth) or intentional (doping).

When an electron (or hole) is trapped in the defect, a hole (or electron) can move into that created state with less energy than would be required for it to cross all the way into the conduction band. If recombination does not occur, the electron (or hole) will be thermally re-emitted back into the conduction (valence) band. This is the dominant mechanism in doped indirect band gap materials like silicon.

The recombination rate is dependent on where in the forbidden gap the defect is introduced. Defects introduced near the conduction band (or valence band) edge are less likely to cause recombination because the electron (or hole) has a higher chance of just being re-emitted into the conduction band (or valence band) than recombining with a hole (or electron) that jumps into the defect energy state. It turns out that traps near the center of the band gap or mid-gap lead to higher Shockley-Read-Hall recombination rates.

If the traps near the band edges are neglected then the SRH lifetime equation can be simplified to Eq. (4) for p-doped materials, and Eq. (5) for n-doped materials: [11]

$$\tau_{SRH} = \tau_{n0} + \tau_{p0}\frac{\Delta n}{\Delta n + N_A} \quad (4)$$

$$\tau_{SRH} = \tau_{p0} + \tau_{n0}\frac{\Delta p}{\Delta p + N_D} \quad (5)$$

Where N_A and N_D are the acceptor and donor doping respectively and Δn and Δp are the carrier injection levels.

1.1.3 Auger Recombination

Auger recombination is basically band to band recombination but instead of the energy given off as a photon, the energy is transferred to the third particle, an electron in the conduction band. That electron's energy then dissipates throughout the conduction band. This is the fastest of the recombination mechanisms in heavily doped materials/high carrier concentration materials because the Auger recombination rate is directly related to the square of the doping concentration. [15]

If the Auger recombination is faster than the other two recombination mechanisms, it will limit the minority carrier lifetime. In electron-electron-hole interactions the recombination process will be proportional to n^2p and for electron-hole-hole interactions the recombination process will be proportional to np^2 where n and p are the total concentrations of electrons and holes respectively.

$$R_{Auger} = Cn^2p \ (6)$$

$$R_{Auger} = Cnp^2 \ (7)$$

If $N_A >> N_D$ (the acceptor doping is much greater than the donor doping) as is the case in heavily doped p-type semiconductors, the above equations produce Eq. (8) for Auger minority carrier lifetime. If $N_D >> N_A$ (the donor doping is much greater than the acceptor doping) as is the case in heavily doped n-type semiconductors, Eq. (9) is obtained for Auger minority carrier lifetime.

$$\tau_{Auger} = \frac{1}{CN_A^2} \ (8)$$

$$\tau_{Auger} = \frac{1}{CN_D^2} \ (9)$$

In Eqs. (8) and (9) C is the auger coefficient. The value of C for silicon is typically given as: $1.66 \times 10^{-30} cm^6/s$ [16] [17].

Since the recombination energy dissipates throughout the material, it is sometimes referred to as thermal recombination and is one of the sources of waste heat in semiconductors.

In the case of low level injection (where the number of minority carriers is much less than the doping) the recombination rate is related to the minority carrier lifetime by the following equation:

$$R = \frac{\Delta n}{\tau} \quad (10)$$

In the above equation R is the recombination rate, τ is the minority carrier lifetime, and Δn is the excess minority carrier concentration.

1.2 Surface Recombination

The effective minority carrier lifetime is a function of the lifetimes of both the bulk and the surfaces. [12] The bulk lifetime can be calculated from Eq. (1) above. The equation for this relation can be seen below.

$$\frac{1}{\tau_{eff}} = \frac{1}{\tau_{bulk}} + \frac{1}{\tau_{surface}} \quad (11)$$

The surface recombination of a semiconductor is an important parameter because the surface is a disruption of the semiconductor crystalline structure as seen in Figure 1.

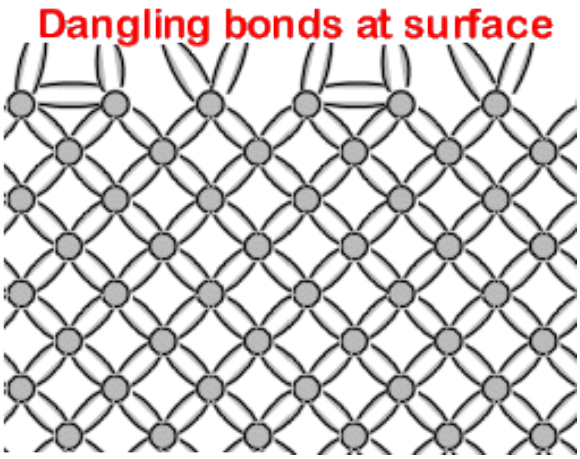

Figure 1: Dangling bonds at the surface of a tetrahedrally bonded material. Source: pveducation.org

A semiconductor crystalline lattice is normally periodic, but at the surface interruptions in the periodicity cause dangling bonds. The number of dangling bonds is directly related to the surface recombination rate. The decrease in the number of dangling bonds decreases the surface recombination rate thus increasing the lifetimes of the minority carriers. Surface passivation is defined as the reduction of dangling bonds on the surface. An example of natural surface passivation is the thin layer of silicon dioxide that forms on a silicon wafer.

The surface recombination is a function of the surface recombination velocity and the thickness. [13] The minority carrier lifetime at the surface of a silicon wafer or thin film is then:

$$\tau_{surface} = \frac{W}{2S} \quad (12)$$

Where S is the surface recombination velocity and W is the thickness of the wafer. The full equation for the effective minority carrier lifetime is then:

$$\frac{1}{\tau_{eff}} = \frac{1}{\tau_{SRH}} + \frac{1}{\tau_{rad}} + \frac{1}{\tau_{Auger}} + \frac{2S}{W} \quad (13)$$

Chapter 2

Photoluminescence Theory

Since photoluminescence occurs in direct band gap materials, radiative recombination is the mechanism that dominates the recombination process. The radiative recombination of free electrons and free holes was given in Eq. (3) above as

$$R_{rad} = B(n_0 + \Delta n)(p_0 + \Delta p) \quad (3)$$

The radiative recombination coefficient, B, is specific to the semiconductor. B is determined from the interband transition matrix element at the Γ-point (k=0) of the Brillouin Zone. [18] This causes B to be much larger in direct band gap materials than indirect. [10] The calculated room temperature B coefficient for GaAs is approximately 2×10^{-10} cm^3 s^{-1} [19] [20] and about $1 \times 10^{-15} cm^3 s^{-1}$ for Si.

If Eq. (3) is substituted into Eq. (10), the radiative lifetime can be written as

$$\tau = \frac{\Delta n}{B(n_0 + \Delta n)(p_0 + \Delta p)} \quad (14)$$

For p-type materials, if the semiconductor is assumed to be in low-level injection, $p_0 >> n_0$ and $\Delta p << p_0$. Also for n -type materials in low-level injection: $n_0 >> p_0$ and $\Delta n << n_0$. [9] If

N is substituted in for the majority-carrier density for a p-type material, the following equation is obtained.

$$\tau = \frac{\Delta n}{B(\Delta n)(N + \Delta n)} \quad (15)$$

If we consider the Δn to be negligible, since $\Delta n << n_0$ and $\Delta n = \Delta p$, the equation simplifies to

$$\tau = \frac{1}{BN} \quad (16)$$

If the effects of SRH and Auger recombination are negligible, the minority carriers should theoretically decay with the radiative lifetime of 1/(BN). [10]

2.1 Generation of electron-hole pairs

The absorption of light by a material can modeled by the following equation

$$I = I_0 * e^{-\alpha x} \quad (17)$$

Where x is the distance into the material at which the light intensity is being calculated, I_0 is the light intensity at the surface of the material, and α, the absorption coefficient, is

related to the extinction coefficient (κ) by the following formula [21] where λ is the wavelength.

$$\alpha = \frac{4\pi\kappa}{\lambda} \quad (18)$$

If it is assumed that every absorbed photon generates an electron-hole pair, Eq. (17) above can be modified to obtain Eq. (19) below. The generation rate, G, of electron-hole pairs at any distance into the sample can be modeled by the following equation:

$$G = \alpha N_0 e^{-\alpha x} \quad (19)$$

In Eq. (19) N_0 is the photon flux at the surface (photons/unit-area/sec.) To obtain the generation of electron-hole pairs through the entire sample Eq. (19) is integrated over x (the thickness of the sample) to become Eq. (20).

$$G_0 = \alpha N_0 \int_0^x e^{-\alpha x} dx \quad (20)$$

The excess carrier concentration is equal to the generation rate multiplied by the minority carrier lifetime. [13]

$$\Delta n = G_0 * \tau_{effective} \quad (21)$$

The light generated from photoluminescence is related to the radiative recombination. The frequency of luminescence light, ν, multiplied by the Planck's constant, h, equals the photon energy. This will be equal to the band gap of the material since radiative recombination is direct band to band recombination.

$$I_{PL} = \int_V R * h\nu \ dV \ (22)$$

If Eq. (11) is substituted for R, Eq. (22) becomes,

$$I_{PL} = \int_V \frac{\Delta \mathrm{n}}{\tau_{rad}} * h\nu \ dV \ (23)$$

This means that if τ_{rad} dominates and $\tau_{effective}$ is roughly equal to τ_{rad}, then a good amount of the absorbed light is released as photoluminescence. If τ_{nr} dominates and $\tau_{effective}$ is much shorter than τ_{rad}, then not much of the absorbed light is released as photoluminescence. If Eq. (13) is simplified so as to model the effective lifetime as a function of the radiative and non-radiative lifetimes, Eq. (24) is obtained.

$$\frac{1}{\tau_{eff}} = \frac{1}{\tau_{rad}} + \frac{1}{\tau_{nr}} \ (24)$$

Transform this equation [18] to get

$$\tau = \frac{\tau_{rad} * \tau_{nr}}{\tau_{rad} + \tau_{nr}} \quad (25)$$

This demonstrates that the minority carrier lifetime will always be shorter than the smaller of the radiative and non-radiative recombination lifetimes. If the non-radiative recombination lifetime is significantly shorter than the radiative recombination lifetime, the effective minority carrier lifetime will also be significantly shorter than the radiative recombination lifetime. This causes the PL intensity to be negligible.

The quantum efficiency is the ratio of the radiative recombination rate to the total recombination rate [14] [22] as seen in Eq. (26). When Eq. (10) is applied it can be seen that the quantum efficiency is inversely proportional to the ratio of the radiative and non-radiative lifetimes (Eq. (27)).

$$\eta_{qu} = \frac{R_{rad}}{R_{total}} \quad (26)$$

$$\eta_{qu} = \frac{1}{1 + \frac{\tau_{rad}}{\tau_{nr}}} \quad (27)$$

If the radiative recombination lifetime is significantly shorter than the non-radiative recombination lifetime, the quantum efficiency approaches unity, and much of the absorbed light is released as photoluminescence.

2.2 Photoluminescence Spectroscopy

Photoluminescence Spectroscopy is a method of measuring electron-hole recombination by measuring the light emitted in direct band to band recombination. In steady state photoluminescence measurements a continuous wave (CW) laser is incident onto a direct band gap semiconductor material such as GaAs. The semiconductor absorbs the light generating excess electron-hole pairs. The electron-hole pairs then recombine and light is re-emitted in the form of a photon near the band gap energy.

In photoluminescence spectroscopy a semiconductor is usually excited by a laser with photon energy considerably above the band gap, and the photoluminescence is detected by a spectrometer. The intensity is then recorded as a function of the photoluminescent wavelength.

Photoluminescence spectroscopy is helpful to quantify and qualify information about the band structure of the material being analyzed. Photoluminescence spectroscopy gives the researcher information about the material such as its band gap, whether it's monocrystalline, polycrystalline, or amorphous, and whether it has a large congregation of trap states. If the material is a crystal, the photoluminescence spectrum will be narrow, whereas an amorphous material will have a wider photoluminescence spectrum. If a material has many trap states, they will show up in the PL spectrum as either narrow or wide signals depending on how concentrated they are in the energy domain. Photoluminescence is a good tool to use in conjunction with other measurement techniques because it is contactless, eliminating the need for an ohmic contact.

The major disadvantage in using photoluminescence is that only direct band gap semiconductors luminesce with enough intensity to be applicable. In addition, if non-radiative recombination mechanisms such as SRH or Auger recombination are dominant in a direct gap material, one will not get photoluminescence. Another problem that must be overcome is that the intensity of photoluminescence is usually very small. This is usually solved by taking multiple measurements and integrating them over time.

2.3 Interference Effects

An issue that can occur in photoluminescence studies of thin films of amorphous and polycrystalline materials is the emergence of interference fringes in the photoluminescence spectra. This is due to the thickness of the films being measured. Bragg's law [23] states that:

$$2dsin(\theta) = m\lambda \quad (28)$$

In Bragg's equation d is the distance between two planes, θ is the angle of incidence, m is a positive integer, and λ is the wavelength of light. For thin films this principle is applied to derive the equations below where n is the index of refraction of the thin film, d is the thickness of the film, θ is the angle of incidence of the light on the back side of the film, m is an integer, and λ is the wavelength of light used. If the refractive index of the substrate is less than that of the film the equations for constructive (29) and destructive interference (30) are obtained.

$$2n_{film}dcos(\theta) = (m - \frac{1}{2})\lambda \ (29)$$

$$2n_{film}dcos(\theta) = m\lambda \ (30)$$

If the refractive index of the substrate is greater than that of the film, then the phase of the reflected light will be shifted by 180° at the front and back of the film. This causes the equations for constructive (31) and destructive interference (32) to be

$$2n_{film}dcos(\theta) = m\lambda \ (31)$$

$$2n_{film}dcos(\theta) = (m - \frac{1}{2})\lambda \ (32)$$

This reflective interference was noted by J. Cernogora when studying photoluminescence in amorphous hydrogenated carbon. [24] He noted that if the optical thickness ($d*n_{film}$) was on the order of width of the PL spectrum or larger then interference fringes may be observed. He also noted that such interference fringes can be eliminated by either making a film of optical thickness smaller than the width of the PL spectrum or by roughening the substrate to eliminate reflection interference as was done in [25] and [26]

Chapter 3

Experimental Apparatus - Steady State Photoluminescence

A steady state photoluminescence spectroscopy system was created using a 532 nm green laser (~80 mW). The green light is generated by first exciting an aluminum gallium arsenide (AlGaAs) laser diode (LD) that operates at a wavelength of 808 nm. The AlGaAs LD then pumps a neodymium-doped yttrium aluminum garnet (Nd:YAG) LD. The ND:YAG laser emits light at 1064 nm.

The 1064 nm output is then input into a frequency doubling crystal of potassium titanyl phosphate (KTP). The KTP crystal halves the wavelength to 532 nm. A dielectric mirror that reflects at 1064 nm and transmits at 532 nm is positioned at the end of the laser cavity, and behind the mirror is an infrared filter that filters out any extraneous 1064 or 808 nm light. This IR filter is often omitted in cheaply made laser pointers.

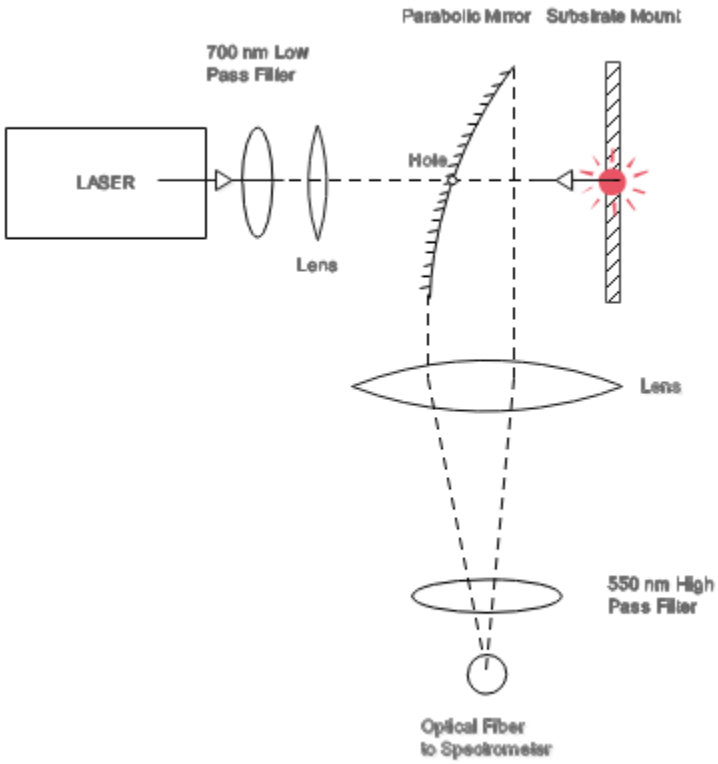

Figure 2: A schematic of the photoluminescence apparatus

Figure 2 above gives a schematic of the photoluminescence apparatus. The laser light is filtered through a 700 nm low pass filter to filter out any stray 808 or 1064 nm light. The filtered light is then focused by a lens through a 0.125 inch hole in a parabolic mirror onto the sample. The illuminated area on the sample can be roughly considered a point so the photoluminescence can be assumed to be radiating as a point source. This radiated luminescence is then captured by the parabolic mirror and focused by a 3 inch diameter lens into an optical fiber. Before reaching the fiber, the light is passed through a 550 nm high pass filter to filter out by the 532 nm laser light.

The fiber is then fed into an Andor Mechelle 5000 spectrometer which utilizes an ICCD camera. The Andor spectrometer has a spectral resolution of .05 nm and can integrate data collected over time. The spectrometer can also account for background radiation and noise.

This photoluminescence apparatus is designed to be modular so that any component can be easily replaced. For example: it was modified to use a 405 nm gallium nitride (GaN) laser (~80 mW). This laser has a two-fold benefit. 405 nm light is of shorter wavelength so it carries more energy per photon than 532 nm light. (3.06 eV as opposed to 2.33 eV) Also the GaN laser diode emits 405 nm without the need of a frequency doubling crystal like the ND:YAG laser. This removes the problem of infrared emission which makes it less dangerous for the human eye because all the radiated light is visible.

It also means that all of the intensity is in the form of 405 nm light. After filtering out the infrared radiation of the 532 nm ND:YAG laser, the output power is only about two thirds of the original power.

The 550 nm high pass filter was also switched out and replaced with a 450 nm high pass filter. This allows the apparatus to measure more of the visible spectrum. One of the problems with using a 405 nm GaN laser is that many materials fluoresce when exposed to this short wavelength light. Among the more common fluorescent materials are paper [27], Scotch tape, laundry detergent, and fibers used in most clothing.

To avoid any problems with extraneous fluorescence, the sample holder, which was originally double sided tape, was replaced with a vacuum sample holder. Also all paper and people were removed from the immediate vicinity of the apparatus. The

experiments were conducted in the dark to avoid interference from the fluorescent bulbs. A picture of the photoluminescence apparatus can be seen below in Figure 3.

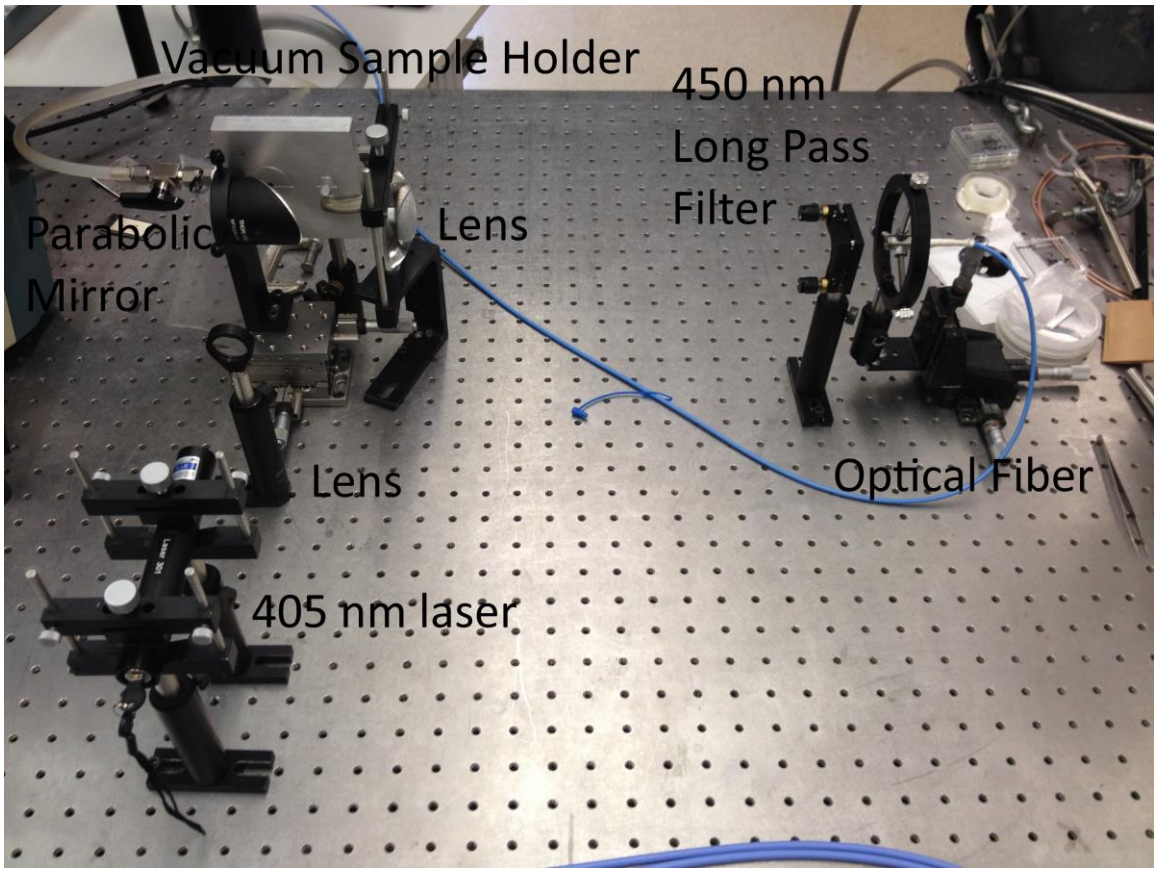

Figure 3: A picture of the PL apparatus using the 405 nm GaN laser, vacuum sample holder, and 450 nm high pass filter.

Some of the materials measured in this thesis are amorphous. Amorphous materials have a characteristic wide photoluminescence spectrum (Section 4.3 or whatever it will be). The transmission as a function of wavelength of the 450 nm long pass filter being used is non-uniform. As can been seen in Figure 4 below, the transmission oscillates between 76% and 94%.

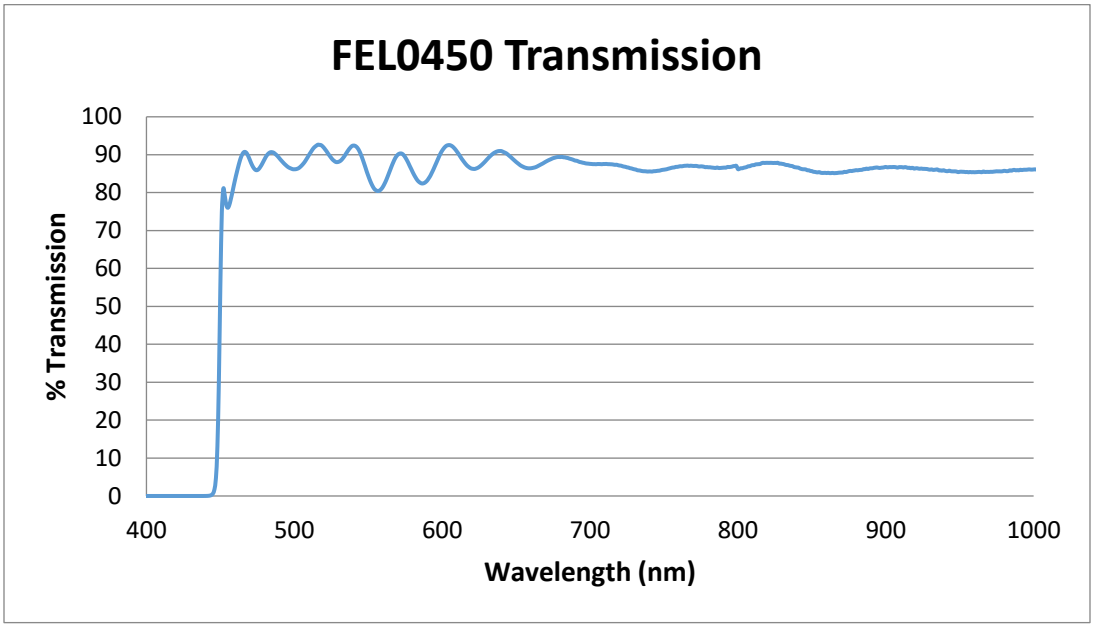

Figure 4: Transmission of the 450 nm long pass filter. Source: Thorlabs

For most materials, particularly single crystals, the photoluminescence spectra are narrow enough that this change in transmission across wavelength is negligible, but the photoluminescence spectra of amorphous materials are broad enough that this difference in transmission can cause erroneous peaks and valleys to appear. The oscillations were accounted for by measuring the transmission of the filter. The photoluminescence data, as measured by the system, was divided by reflection of filter (100% - transmission). The resulting spectrum was then processed as discussed in the next section.

3.1 Data Processing

The data in the form of an intensity vs. wavelength graph is then processed via a Savitzky–Golay filter [28]. A Savitzky-Golay filter is a low pass filter that fits small sub-

sets of data points with a polynomial by the linear least squares method. This increases the signal to noise ratio without distorting the signal. Savitzky and Golay demonstrated that a polynomial can be fit to a set of equally spaced data points and then evaluating the polynomial at a single point within the set produces convolution coefficients for the set of data points. This then produces a smoothed estimate of the original data.

3.2 System Tests

Before using the system to measure the photoluminescence of new materials, the apparatus was tested using materials with known photoluminescence spectra. The three materials used as tests were chromium-doped aluminum oxide ($Cr:Al_2O_3$), gallium arsenide (GaAs), and hydrogenated amorphous silicon (a-Si:H). These materials have all been extensively studied and their photoluminescence spectra are all well known.

3.2.1 Aluminum Oxide

A Cr^{3+} doped aluminum oxide ($Al_{2-x}Cr_xO_3$) ceramic substrate was used for the alignment of the photoluminescence system. Al_2O_3 is a corundum commonly known as sapphire. Cr^{3+} ions are usually found in alumina in nature and manifests itself by a sharp R1, R2 doublet photoluminescence signal at about at 693 and 694 nm. [29] This strong signal is noticeable even at molar concentration below 1 ppm. [30]

Chromium doped aluminum oxide is commonly known as a ruby, and this 694 nm luminescence is what gives rubies their deep red color. The first laser that was developed

was a ruby laser by Theodore H. "Ted" Maiman on May 16, 1960. [31] This ruby laser emits a deep red beam at 694.3 nm.

Because of its intense luminescence signal, and its unique R1, R2 peak, chromium doped aluminum oxide was used as a test sample to confirm that the photoluminescence apparatus was calibrated and working properly. It was also used to align the optical fiber to ensure that the maximum luminescent light was being captured. The data below in figures 9 and 10, taken with the PL apparatus match the data found in the literature. [29] [30] [31] The tall and short peaks are at 694.3 nm and 692.9 nm respectively. The FWHM of the tall and short peaks are 0.85 nm and 0.74 nm respectively. The thin, intense, peaks demonstrate $Al_{2-x}Cr_xO_3$ to be a good example of a polycrystalline material. Figure 5 is a full-spectrum graph, and Figure 6 is zoomed in before and after data processing. It can be observed that the Savitzky–Golay filter does increase the signal to noise ratio without distorting that data. From this point on, unless otherwise stated, the presented data will be processed with the Savitzky–Golay filter.

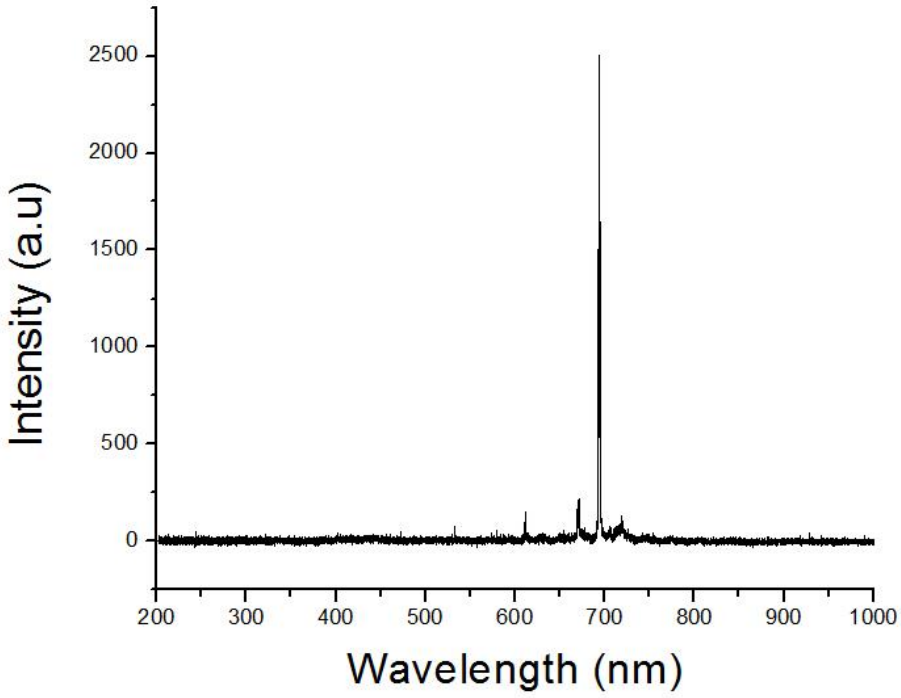

Figure 5: Strong Photoluminescence peak at ~694 nm in Al_2O_3:Cr

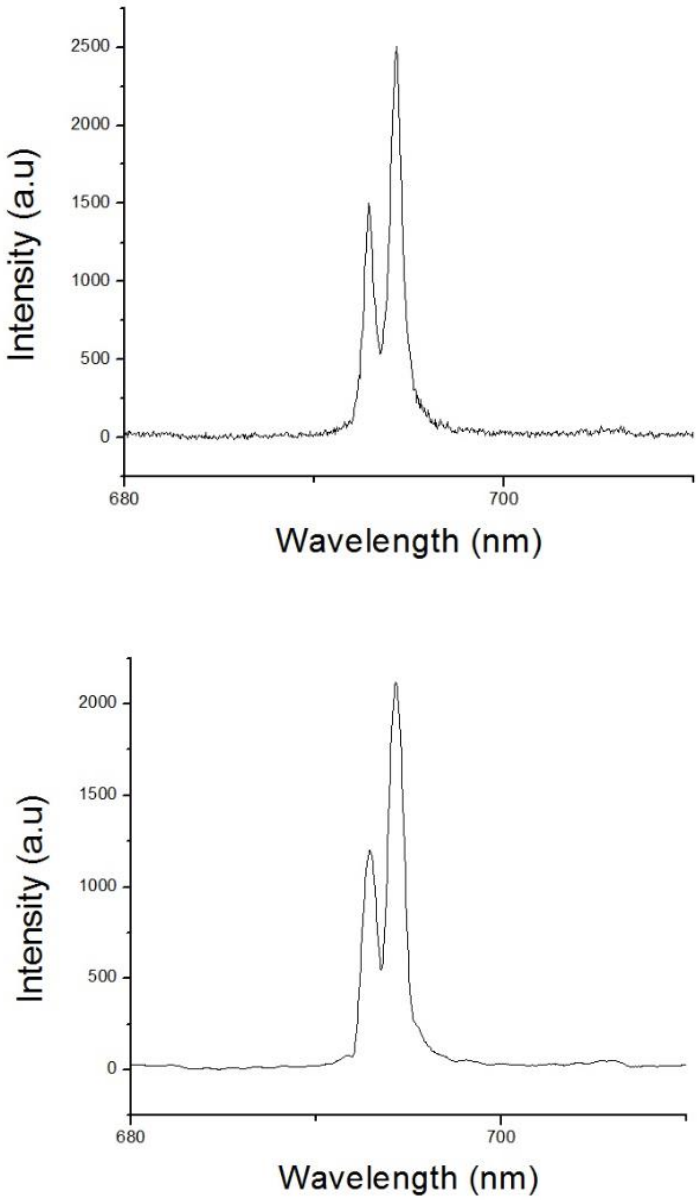

Figure 6: R1, R2 Doublet at 692.9 and 694.3 nm a) before and b) after smoothing

3.2.2 Single Crystal Gallium Arsenide

Gallium arsenide (GaAs) is a well-known single crystal material with a direct band gap of 1.42 eV. Photoluminescence was performed on Zn-doped p-type GaAs with

$p \geq 5*10^{18}$ /cm^3. The resulting spectrum can be seen in Figure 7 below. Three peaks are evident: a small peak at 817 nm, and two more prominent peaks at 846 nm and 871 nm.

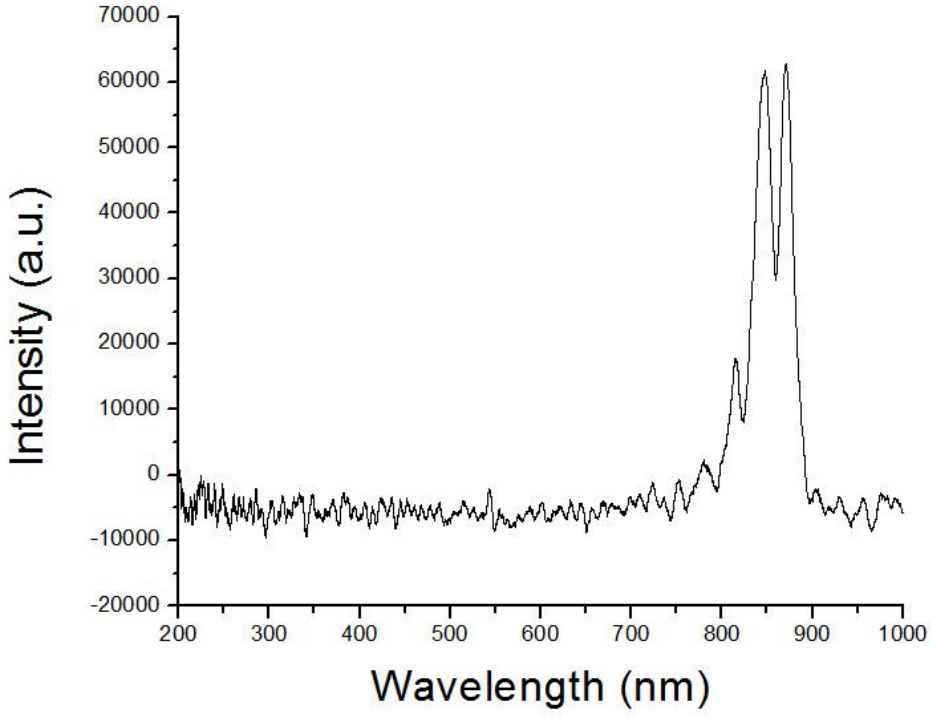

Figure 7: Photoluminescence of p-type GaAs gives three peaks: 817 nm, 846 nm, and 871 nm

The 817 nm peak corresponds to an energy of 1.51 eV which is greater than the band gap. This occurs because the GaAs is degenerately doped. The high concentration of donors causes the Fermi level to fall below the valence band as explained by Wang et. al. and Figure 8. [34] This peak is often seen in photoluminescence measurements of degenerately doped GaAs. [35] [36] [37] At these higher doping levels (greater than 10^{18}/cm^3) the non-radiative recombination increases and the peak due to the modified

Fermi level decreases. This would explain why the 1.51 eV peak is much less intense than the other two peaks.

At 300K (room temperature) the 871 nm peak (1.42 eV) is due to the band to band transition. The band gap of GaAs at room temperature is 1.42 eV. The 846 nm peak (1.46 eV) is believed to be caused by the band to acceptor transition. Because the doping concentration is high, on the order of $5*10^{18}$ /cm^3, the acceptor level is below the top of the valence band rather than in the forbidden gap. Chen et al. noted that this peak was more prominent at higher doping concentrations and higher laser intensities. [33] He stated that the peak was due to the transition between the conduction band and the bottom of the impurity band. At a doping concentration of $5*10^{18}$ /cm^3, the two peaks are of roughly equal intensities. A higher concentration would result in a larger 846 nm peak whereas a lower concentration would result in a larger 871 nm peak.

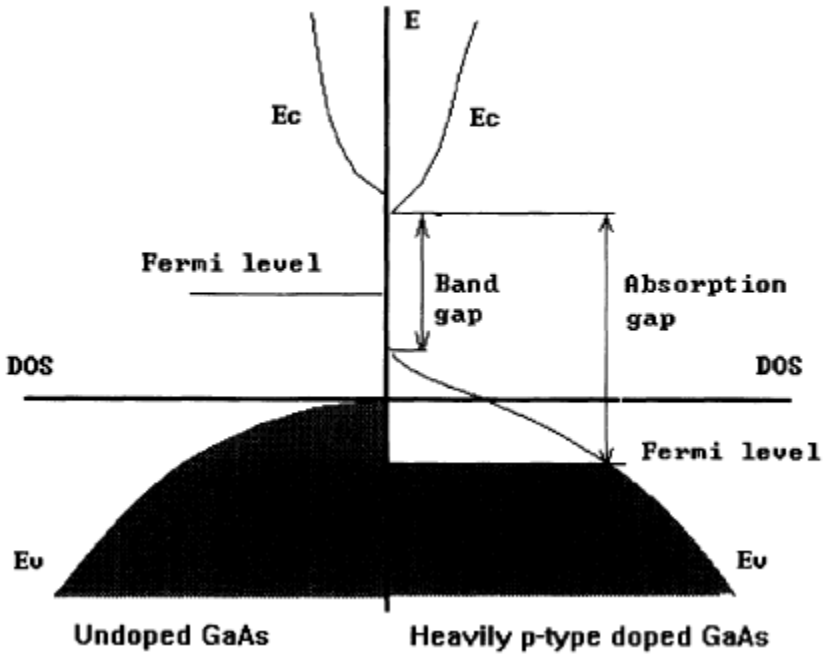

Figure 8: Density of states and position of Fermi level in undoped vs. heavily p-type doped GaAs. Source: Wang et al. [34]

3.2.3 Amorphous Silicon

While crystalline silicon has an indirect band gap of 1.12 eV, hydrogenated amorphous silicon (a-Si:H) has a direct band gap. This direct gap amorphous structure leads to the release of a photon rather than a phonon. In crystalline silicon a phonon is required for the electron to move in k-space to where it can drop into the valence band as seen in the indirect bandgap section of Figure 9 below.

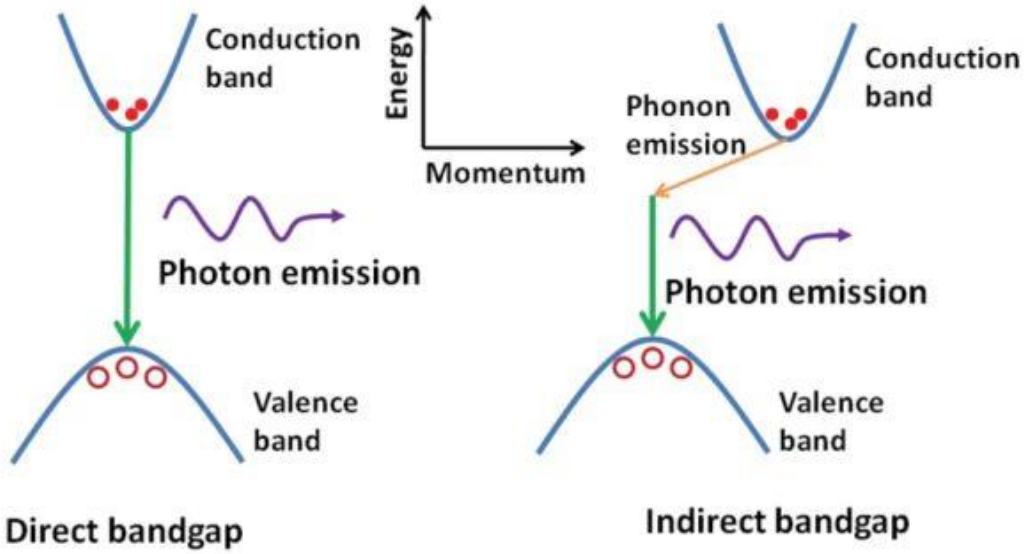

Figure 9: Comparison of electron-hole recombination in direct and indirect band structures. Source: "Advances in Lasers and Electro Optics", Edited by Nelson Costa and Adolfo Cartaxo

Though amorphous solids have no crystalline structure, they are not entirely chaotic. The atomic bond lengths and angles are the same as in crystals and, in the case of silicon, every silicon atom still makes 4 covalent bonds. [38] This means that on a small atomic scale amorphous and crystalline solids behave very similarly. The difference is seen on a larger scale. Since the amorphous solid is not periodic, Bloch's theorem no longer accurately portrays the movement of electrons and holes in amorphous materials.

In 1971 Weaire and Thorpe published two papers calculating the band structure of a tetrahedrally bonded solid regardless of its crystal structure.[39][40] Their model, now called the Weaire-Thorpe model, assumes that the atomic structure is arranged in a near tetrahedral crystal with roughly a 10% perturbation in bond length and angle.

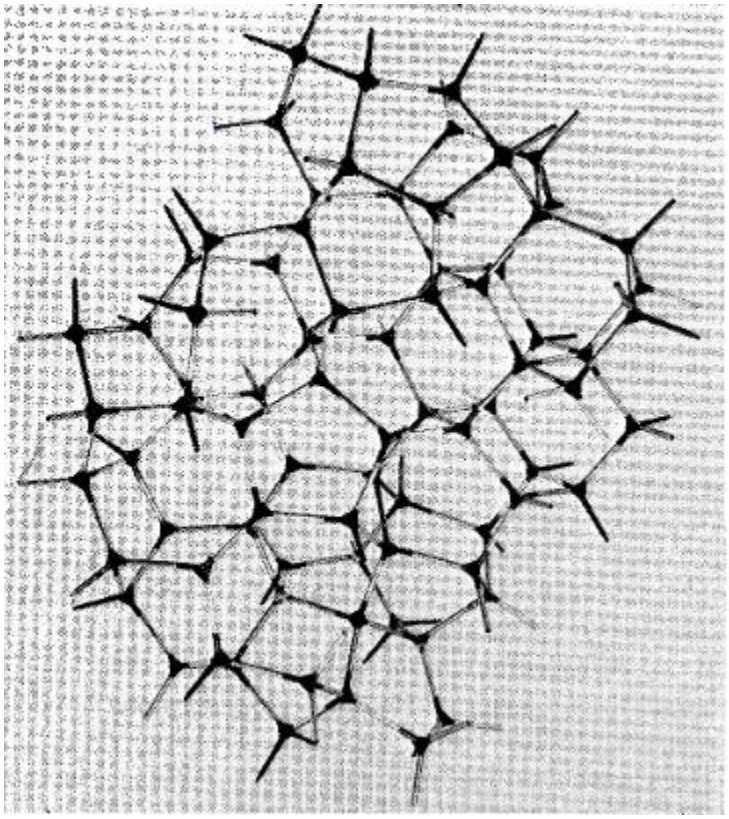

Figure 10: Atomic structure of a solid according to the Weaire-Thorpe model. Source: Weaire and Thorpe 1971

$$H = \sum_{i,j \neq j'} V_1 \left|\phi_{ij}\right\rangle\left\langle\phi_{ij'}\right| + \sum_{i \neq i',j} V_2 \left|\phi_{ij}\right\rangle\left\langle\phi_{i'j}\right| (33)$$

Thorpe and Weaire defined the Hamiltonian seen in Eq. (33) above under the tight-binding approximation so only the four nearest neighbors are considered. [39] V_1 and V_2 are the matrix terms and defined to be real. ϕ_{ij} are the localized wavefunctions for atom index, i, and bond index, j. If V_1 or V_2 are set to zero, then the result is decoupled bonds or atoms with degenerate eigenstates, so Thorpe and Weaire assert that the ratio V_1/V_2 is necessary for determining the band structure.

According to Thorpe and Weaire the band gap is described as the bonding and anti-bonding states of the covalent bond split by the V_2 term and broadened by the V_1 term in the Hamiltonian above. This tight-binding Hamiltonian gives information about the bonding in the short range structure, but not for long range in silicon. Weaire and Thorpe demonstrated that there is a band gap for a certain range of interaction strength V_1/V_2.

The main difference in band structure between amorphous and crystalline solids is that the band edges, which are well defined in a crystal, trail off into the band gap in an amorphous material. There is a non-zero density of states in the forbidden gap [41] (see Figure 11.) This non-zero density of states in the forbidden gap produces a broad photoluminescence spectrum.

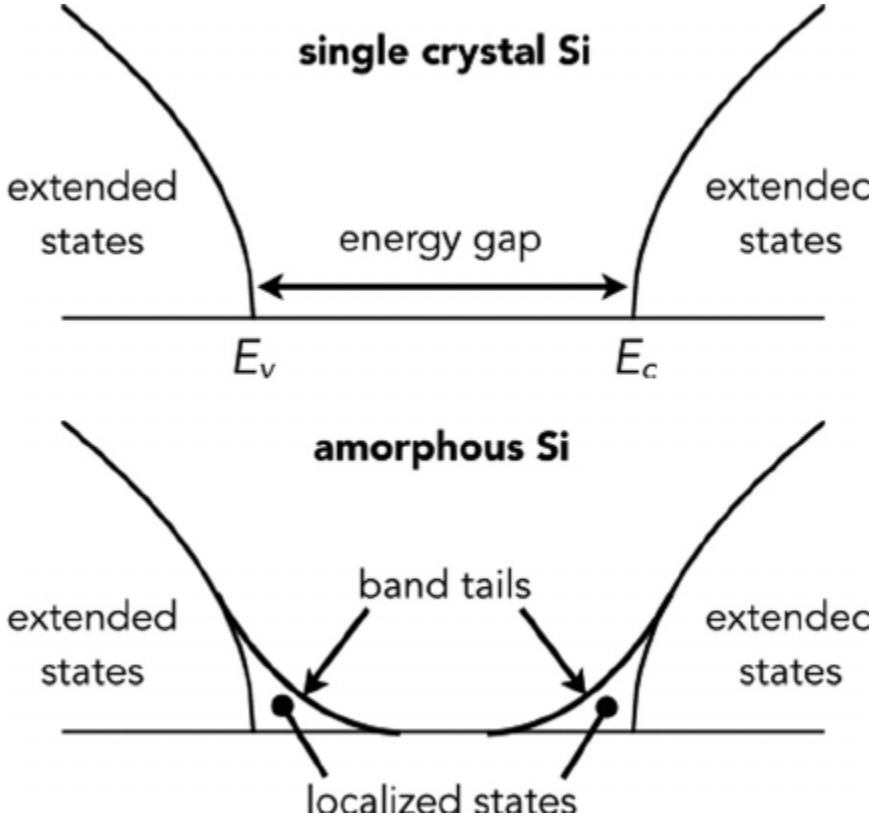

Figure 11: Band edge in crystalline vs amorphous silicon Source: Gilles Horowitz French National Centre for Scientific Research

Hydrogenated amorphous silicon is different from pure amorphous silicon in that it has dangling bonds that have then bonded to a hydrogen atom. The dangling bonds in pure amorphous silicon become holes for electrons to fall into thus diminishing the luminescent photons that could otherwise be emitted from the material. Bonded hydrogen atoms create defect states that are present throughout the band gap [38].

Electrons can fall into these defect states and be trapped for a while without recombining with holes. Because of these defect states, the band gap of a-Si:H is not very well defined. The non-zero density of states allow for a varying distance that excited electrons must traverse to find an unoccupied state either jumping from the valence band

to the conduction band or falling from the conduction band to the valence band. This varying distance leads to a very broad photoluminescence signal ($\Delta\lambda$ ~200 nm). If the material is a single crystal and the bandgap is well-defined, the photoluminescence signal should be very narrow.

Photoluminescence of a hydrogenated amorphous silicon (a-Si:H) solar cell was measured and the spectrum can be seen in Figure 12 below. The structure of the PL signal is in accordance with literature results. [38-41] There is a broad photoluminescence signal ($\Delta\lambda$ ~200 nm) with its peak at 715 nm (1.73 eV) [42].

Hydrogenated amorphous silicon was used as a system test because it is similar to hydrogenated amorphous boron carbide, the material the thesis is attempting to characterize. Both materials are amorphous and passivated with hydrogen. Both materials have a direct band gap and should photoluminesce. Both materials' photoluminescence spectra are expected to be similar in appearance. Amorphous silicon is a well-studied example of an amorphous material.

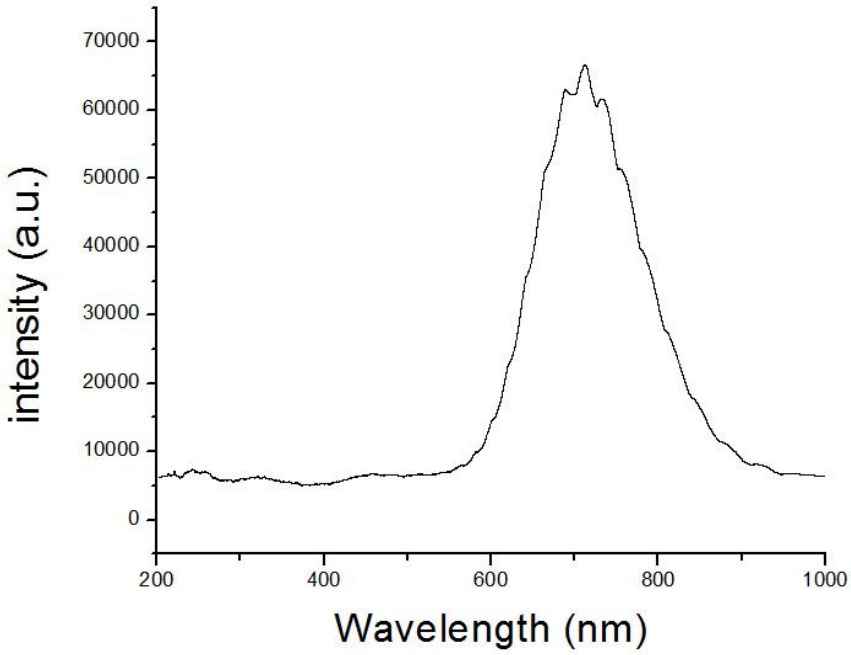

Figure 12: Photoluminescence of a-Si:H gives a broad single peak characteristic of amorphous materials

Chapter 4

Materials Tested

4.1 Amorphous Boron Carbide

One of the materials that was analyzed for this thesis was hydrogenated amorphous boron carbide (a-B_5C:H). Wide ranges of chemical compositions are possible for boron carbide and many of the B_xC_y stoichiometries have been studied intensively for the past two decades. Boron carbide is known to be an atomically hard substance with high temperature stability. While the most abundant and most stable form of boron is ^{11}B, boron carbide is rich in ^{10}B isotopic boron. Boron carbide possesses unique thermoelectric properties [43] that allow for high neutron absorption with little nuclear activity. [44] That along with its self-healing ability has caused it to be of great interest for the nuclear industry.

One of the major research applications of Boron Carbide is the creation of a cheap, portable, solid state neutron detector. This is of great interest for energy, defense, and homeland security. Its ability to detect neutrons comes from the $^{10}B(n, \alpha)^7Li$ neutron capture reactions. This reaction generates lithium atoms of .84 MeV, helium atoms of 1.47 MeV, and a gamma ray of 0.48 MeV 94% of the time. [44]

$$^{10}B + n \rightarrow {}^{7}Li\ (0.84\ MeV) + {}^{4}He\ (1.47\ MeV) + \gamma\ (0.48\ MeV)\ (94\%)$$

$$^{10}B + n \rightarrow {}^{7}Li\ (0.84\ MeV) + {}^{4}He\ (1.78\ MeV)\ (6\%)$$

Since the products of this reaction are known, a solid state neutron detector based on boron carbide only requires cheap and reliable synthesis of boron carbide. The BC films analyzed for this thesis were fabricated via plasma-enhanced chemical vapor deposition (PECVD) for the solid precursor orthocarborane (1,2-$C_2B_{10}H_{12}$, 1a). This method has been shown to reliably reproduce high-resistivity (10^{10}–10^{13} Ω cm) films of device quality [45-47].

Another application for boron carbide is a neutron-voltaic cell. A boron carbide p-n junction under neutron flux behaves similarly to a standard p-n junction solar cell as seen in Figure 13 below. The only difference is that in this case there is a nuclear reaction. A neutron is absorbed by the device and reacts with the ^{10}B producing helium atoms with energies of 1.47 MeV. The ejected helium can then create electron-hole pairs in the boron carbide p-n junction. The charge carriers can be captured by the junction's internal electric field resulting in current flow.

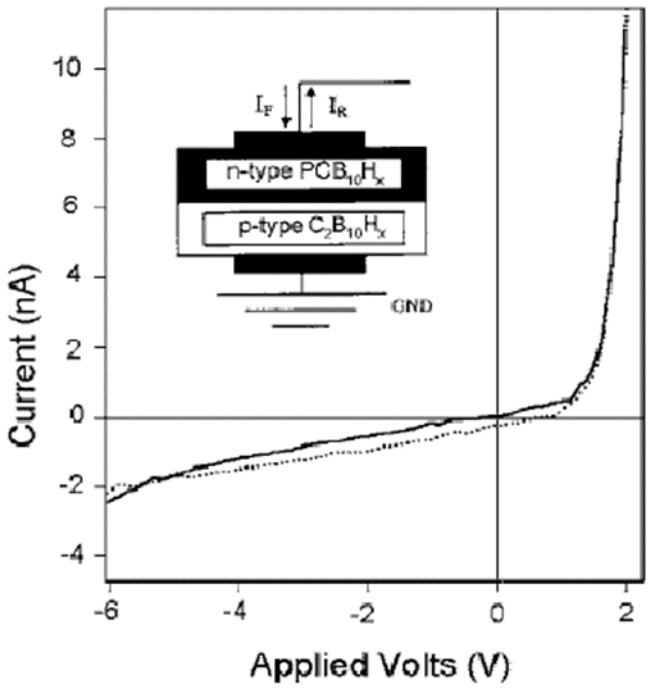

Figure 13: The I-V Curve of boron carbide under neutron radiation Source: S. Balaz, D. I. Dimov, N. M. Boag, K. Nelson, B. Montag, J. I. Brand, P. A. Dowben, Appl. Phys. A (2006)

4.2 Tungsten Diselenide

Another material that was measured using photoluminescence spectroscopy was tungsten diselenide (WSe_2). Tungsten diselenide along with materials such as tungsten disulfide (WS_2), molybdenum disulfide (MoS_2), and molybdenum diselenide ($MoSe_2$) are called transition metal dichalcogenides (TMCs). Transition metal dichalcogenides are materials that consist of one of the 15 transition metals and one of the three chalcogenides. Chalcogenides consist of sulfur, selenium, or tellurium.

Transition metal dichalcogenides are layered 2-dimensional materials with each layer bonded together by the van-der-Waals interaction. As seen in Figure 14 below, a

layer of tungsten diselenide is made up of a tungsten layer sandwiched between two selenium layers. A thin film is made up any number of these layers stacked on top of each other.

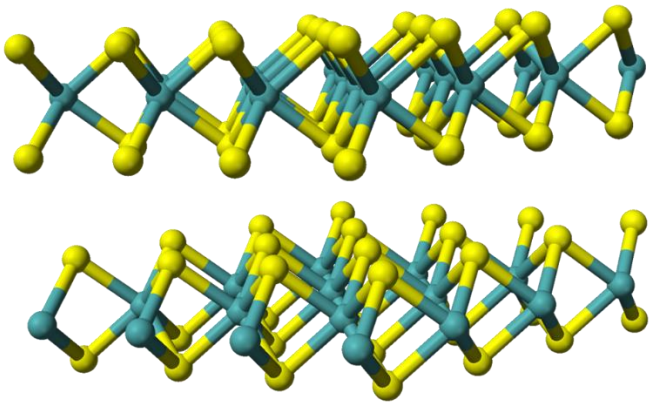

Figure 14: Two Layers of Tungsten Diselenide (WSe_2) Source: Wikipedia

The length of the tungsten-selenium bond is about 0.2526 nm, and the length of the selenium-selenium bonds is 0.334 nm. [48] Bulk tungsten diselenide has both a direct and an indirect band gap whereas a single monolayer has a direct band gap. [49] A quick search of "WSe_2" and "photoluminescence" on Web of Science did not bring up any results where the WSe_2 samples were thicker than 20 nm. [50]

Monolayer and few monolayer Tungsten diselenide as well as other transition metal dichalcogenides have quickly become an important research topic because of their 2-D graphene-like nature. Like graphene, single layers of WSe_2 have a very high electron mobility, but unlike graphene, which has a zero band gap, monolayer WSe_2 has a high band gap around 1.65 eV. [51]

The most prominent thin film photovoltaic currently is the chalcogenide, Cadmium telluride (CdTe). [52] [53] CdTe laboratory devices have been made with over 15% conversion efficiency, and large area modules have been made with over 9% efficiency. While CdTe shows promise for the solar cell industry, the main drawbacks are that cadmium is toxic and tellurium is rare. [54] Tungsten diselenide has been proposed as an alternative because it is safe, earth abundant, and has an ideal bandgap for photovoltaics. [55]

It has been shown that with increasing numbers of monolayers the photoluminescence intensity of $MoSe_2$ and WSe_2 decreases considerably. Also, the photoluminescence spectrum moves to lower energies, and a second peak emerges. [50] [51] This second peak is due to the indirect band gap forming. The indirect band gap is smaller than the direct gap at around 1.35 eV. Much research has been done on the photoluminescence of single layer or n-layer WSe_2 where $n<5$, but photoluminescence data has not been recorded on films thicker than 20 nm.

Chapter 5

Results

5.1 Amorphous Boron Carbide Results

The boron carbide films are amorphous and hydrogenated (a-B_5C:H) causing them to have similar characteristics to hydrogenated amorphous silicon (a-Si:H) in that they have a direct, but not well-defined, band gap. Photoluminescence spectroscopy lends itself as a good tool to characterize these boron carbide samples because of its ability to measure intensity of luminescence as a function of wavelength. This can give us information about the width of the band gap and to what extent the band tails extend into the forbidden gap. Photoluminescence is also ideal because it is contactless and non-destructive to the films.

Our research team is able to synthesize hydrogenated amorphous boron carbide (a-B_5C:H) with direct band gaps ranging from 1.55 eV to 2.11 eV measured by the ellipsometrically determined Tauc plot method by varying the deposition temperature, pressure, and power applied to the electrodes. This ability combined with an organic linker molecule [56] (Bis-BN Cyclohexane) gives a large degree of control over the

optical and electronic properties of boron carbide material that can be created. A graph of the absorption of some of the materials can be seen in Figure 15 below.

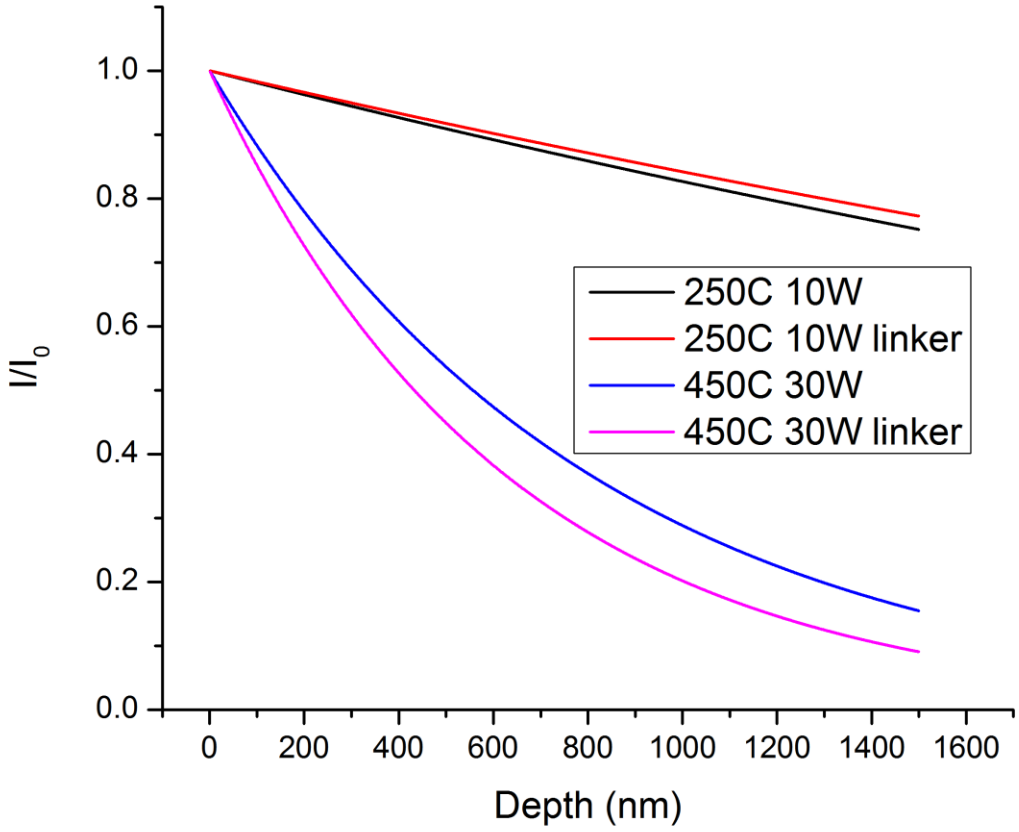

Figure 15: Absorption curve at 405 nm light of a-B5C:H with high band gap (blue and purple lines) and low band gap (red and black lines) both with and without the linker molecule. Determined by ellipsometry

The absorption of monochromatic light can be modeled by the Beer-Lambert Law seen in Eq. (34) below is an extension of Eq. (17) [57] where x is the depth of the sample,

x_0 is where the light starts being absorbed, I(x) is the light intensity at depth x, and α is the absorption coefficient.

$$I(x) = I(x_0) * e^{\alpha(x-x_0)} \quad (34)$$

The absorption coefficients for the highest and lowest band gap boron carbide along with the organic linker molecule are given in Table 1 below.

Table 1: Absorption coefficients of high and low temperature boron carbide samples

	405 nm	532 nm
250C	0.000190388 nm^{-1}	99.6805 cm^{-1}
250C linker	0.000172113 nm^{-1}	101.57 cm^{-1}
450C	0.00124407 nm^{-1}	1949.44 cm^{-1}
450C linker	0.001601171 nm^{-1}	3438.03 cm^{-1}

In the photoluminescence experiments performed for this thesis the angle of incidence is 0º, the thickness of the boron carbide films was ~1 μm, and the index of refraction was ~1.9-2.2 [58] which is less than the silicon substrate. These films may yield interference fringes in the PL spectrum as discussed in section 2.3. In order to address this issue thinner films (~200 nm) were deposited. To avoid interference fringes the sample must be thinner than Eqs. (35) and (36) for constructive and destructive interference respectively.

$$d = \frac{\lambda}{2n_{film}} \quad (35)$$

$$d = \frac{\lambda}{2 * 2n_{film}} \quad (36)$$

As can be seen in Figure 16 the PL spectrum of amorphous boron carbide bears a resemblance to amorphous silicon. Both materials have a broad PL curve ($\Delta\lambda$ ~200 nm) that can be modeled as a single Gaussian distribution. Also they both peak in the red area of the visible spectrum. The peak of the signal gives us the band gap, [59] and the width gives us a qualitative idea of the extent to which the band tails extend into the forbidden gap. In amorphous materials the broader the PL spectrum is, the more chaotic (less crystalline) the material is.

The amorphous hydrogenated boron carbide was synthesized via plasma-enhanced chemical vapor deposition (PECVD). The deposition parameters that were analyzed for this thesis were temperature, and the power applied to the electrodes. As temperature and power were increased, the band gap decreased. The largest band gap measured was 2.04 eV for a deposition temperature of 250ºC at 10 Watts, and the smallest band gap measured was 1.86 eV for a deposition temperature of 450ºC at 30 Watts. A table of the samples' deposition temperature, power, band gap as determined from photoluminescence, band gap as determined from the ellipsometrically determined Tauc plot method, and the full width at half maximum (FWHM) of the photoluminescence spectra is presented below.

Table 2: Band gaps as a function of deposition parameters

Temperature	Power	Band Gap PL	Band Gap Tauc Plot	FWHM PL
250 ºC	10 W	2.04 eV	2.11 eV	207 nm
250 ºC	30 W	1.92 eV	1.96 eV	208 nm
450 ºC	10 W	1.91 eV	1.65 eV	234 nm
450 ºC	30 W	1.86 eV	1.55 eV	214 nm

A graph of the PL spectra at the four different temperatures and powers overlaid can be seen in Figure 16 below. It can be seen from Table 2 that the temperature and power do not seem to affect the width of the photoluminescence curve indicating that crystallinities of the boron carbide samples are all similar.

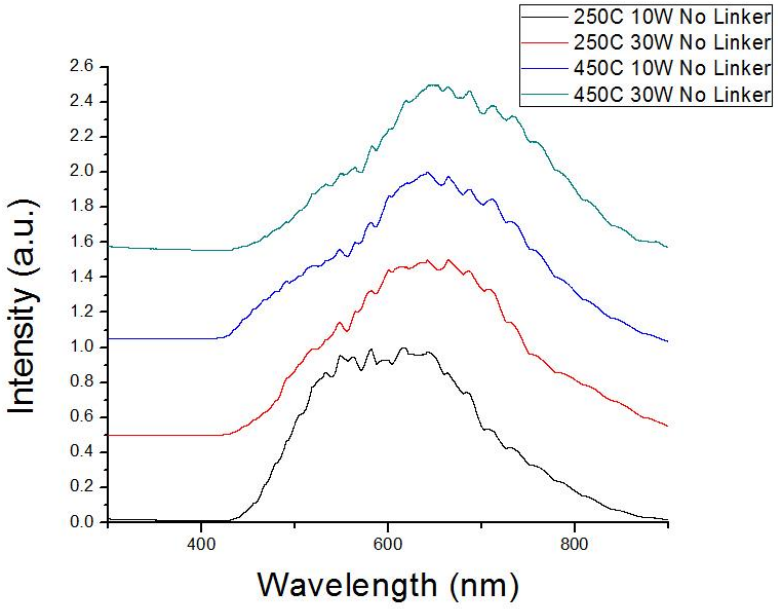

Figure 16: As deposition temperature and power increase band gap decreases

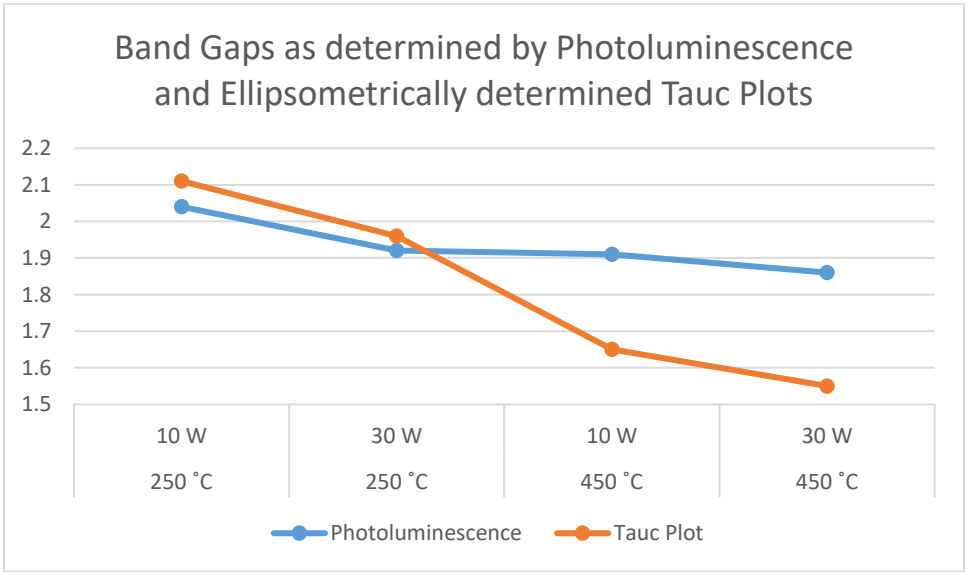

Figure 17: Band gaps determined by photoluminescence compared with that of those determined by ellipsometry. It can be seen that both methods show that band gaps decreasing as deposition temperature and power increase, but ellipsometry shows a more substantial decrease in band gap.

In Figure 17 it can be seen both the photoluminescence measurements and the ellipsometry measurements so a decrease in band gap as deposition temperature and power increase. But it must be pointed out that while the band gaps as determined from PL and ellipsometry are consistent for the lower temperatures, they differ more for the higher temperatures. This is assumed to be because between 200ºC and 300ºC the temperature is optimal for hydrogen passivation. [60] At higher temperatures hydrogen starts to be driven out of amorphous materials. This leaves dangling bonds that can hold electrons.

These dangling bonds, as in the case of surface recombination, create trap states that can trap carriers. These trap states could allow for the boron carbide to absorb low intensity light below its actual band gap producing a Tauc plot with a lower band gap. Photoluminescence measurements, on the other hand, are the result of high intensity absorption. When relaxing, electrons will either fall into the valence band (radiative recombination) or into one of the traps caused by dangling bonds (Shockley-Read-Hall recombination). In the case of SRH recombination no light is emitted. Photoluminescence is an emission measurement so it doesn't measure the non-radiative recombination, producing what looks like a higher band gap.

These two measurements together give information regarding the band structure of amorphous boron carbide. They tell us that at 250ºC the band edges behave like a well-understood amorphous material, but that at 450ºC the band edges are more incoherent and there is discrepancy between absorption and emission.

5.2 Tungsten Diselenide Thin Film Results

Since tungsten diselenide has promising solar cell properties photoluminescence spectroscopy is a great tool for understanding its band structure, defects and overall assessment of film quality.

Our research team is able to synthesize WSe_2 films of varying thicknesses. This is done via sputtering deposition of tungsten onto quartz and then processes the tungsten film in a selenium atmosphere to convert it to WSe_2. Typically the samples are then processed at 875º C for 12 hours. This time and temperature allow for the tungsten and selenium to react and for annealing to occur.

This process leads to the films thickness increasing by roughly a factor of four. This process is safe and reproducible and can be used to create WSe_2 films anywhere from 100 nm to 500 nm. These films have a recorded mobility of 30 cm2/Vs, but unfortunately no photoluminescence was detected.

This is assumed to be because at 100 nm and thicker, these films are much thicker than what is considered a bulk WSe_2 material. Bulk WSe_2 has both a direct and an indirect band gap, but the indirect gap is smaller (1.35 eV as compared to 1.65 eV) this means that there is a much larger probability that the recombination will be phonon-assisted and the radiative recombination coefficient will be much less than in direct gap transitions.

Arora et. al. [50] noticed that a single monolayer of tungsten diselenide gave a bright photoluminescence signal at about 1.65 eV but at a thickness of 20 nm the peak had shifted to about 1.25 eV and the intensity had dropped by a factor of 10000 (see

Figure 18). This decrease in PL energy corresponds to the shift from the direct band gap to the indirect band gap. The decrease in PL intensity makes sense when comparing the radiative recombination coefficients of silicon and gallium arsenide. The radiative recombination coefficient for silicon is about five orders of magnitude less than that of gallium arsenide. [19] [20]

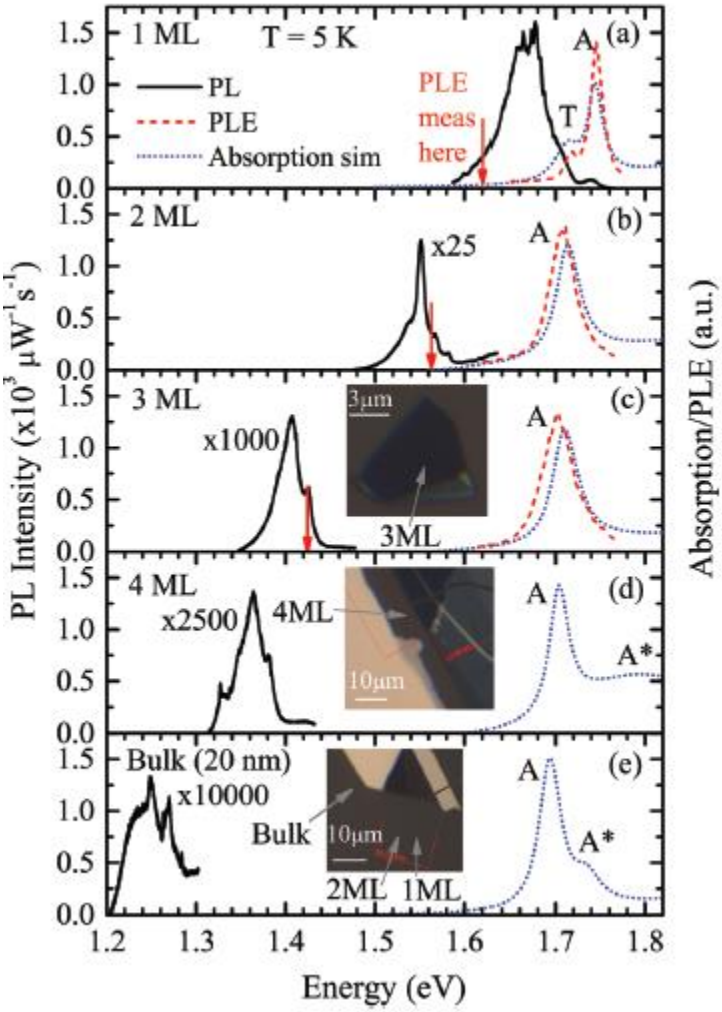

Figure 18: Photoluminescence and PLE of 1, 2, 3, and 4 monolayers, and bulk (20 nm) of tungsten diselenide. Source: Arora et. al.

Chapter 6

Conclusions and Future Work

This thesis has discussed photoluminescence theory as well as document the building of a modular photoluminescence system. Testing of this apparatus was completed using three materials of differing crystallinity. Chromium-doped aluminum oxide ($Cr:Al_2O_3$) was used as a system test for polycrystalline material. It was also used to test the system's wavelength calibration. Gallium arsenide (GaAs) was also used as a single crystal test material for the apparatus. The last material to be used as a system test was hydrogenated amorphous silicon (a-Si:H). The photoluminescence apparatus was tested on amorphous silicon to determine its efficacy with amorphous materials. The photoluminescence apparatus behaved as expected with all system tests.

After it was demonstrated that the photoluminescence apparatus worked as expected, it was used to characterize two new materials, hydrogenated amorphous boron carbide ($a\text{-}B_5C:H$) and tungsten diselenide (WSe_2). It was shown in this thesis that boron carbide thin films produced by plasma enhanced chemical vapor deposition (PECVD) are indeed amorphous and have a direct band gap. It was also shown that the band gap decreases with increased deposition temperature and plasma power supply power. Neither one of these deposition parameters had a noticeable effect on the width of the photoluminescence curve.

6.1 Future Work

There are many way this research can continue. Firstly, the photoluminescence apparatus is modular so any part can be changed out for a different/higher quality part. For example, the laser could be swapped out for one with shorter wavelength or higher intensity. Or the long pass filter could be swapped for one with a flat transmission curve.

The future plans for research into amorphous boron carbide include determining what effect changing the deposition pressure and the choice of plasma has on the photoluminescence signals. Also there are plans to create a multi-dimensional matrix of the extreme values of the deposition parameters to obtain a better idea of how they work together to affect the band structure of boron carbide. Currently the introduction of an organic linker molecule (Bis-BN Cyclohexane) is being attempted. Research in being done to determine how this linker molecule affects the optical and electron properties of the boron carbide.

Other future plans are to create thinner tungsten diselenide films. Once thinner films can be reproduced reliably, photoluminescence will be taken on the films to measure the intensity as a function of thickness. Photoluminescence will also be used to look into how the recombination shifts from the direct band gap to the indirect band gap as film thickness increases.

References

[1] G. Busch, “Early history of the physics and chemistry of semiconductors – from doubts to fact in a hundred years”, Eur. J. Phys., vol. 10, no. 4, pp. 254–263, 1989.

[2] W. Mönch, *Semiconductor Surfaces and Interfaces*. Berlin-Heidelberg: Springer, 2001.

[3] A.E Becquerel Comt. Rend. Acad. Sci., 9 (1839), p. 561

[4] Z. A. Smith and K. D. Taylor, *Renewable and Alternative Energy Sources: A Reference Handbook*. Santa Barbara: ABC-CLIO Inc., 2008, p. 157.

[5] L. Hoddeson, E. Braun, J. Teichmann, and S. Weart, *Out of the Crystal Maze: Chapters in the History of Solid State Physics*. New York: Oxford University Press, 1992.

[6] Brattain W H and Bardeen J 1953 Surface properties of germanium Bell Syst. Tech. J. **32** 1–41

[7] Garrett C G B and Brattain W H 1955 Physical theory of semiconductor surfaces Phys. Rev. **99** 376–87

[8] *UV-VIS and Photoluminescence Spectroscopy for Nanomaterials Characterization.* edited by Challa S. S. R. Kumar. Berlin Heidelberg: Springer-Verlag, 2013.

[9] W. K. Metzger, R. K. Ahrenkiel, P. Dippo, J. Geisz, M. W. Wanlass, S. Kurtz, NREL/CP-520-37028, January 2005

[10] R. Ahrenkiel, *Solid-State Electronics* Vol. 35, No. 3, pp. 239-250, 1992

[11] D. K. Schroder, *Carrier Lifetimes in Silicon.* IEEE Transactions on Electron Devices, vol. 44, no. 1, January 1997

[12] O. Palais “High resolution lifetime scan maps of silicon wafers”, Materials Science and Engineering B71 (2000) 47–50

[13] Andres Cuevas, Daniel Macdonald, “Measuring and interpreting the lifetime of silicon wafers, Solar Energy”, Volume 76, Issues 1-3 (2003) 255-262

[14] Semiconductor Laser Theory By Prasanta Kumar Basu, Bratati Mukhopadhyay, Rikmantra Basu pages 197-202

[15] Organic Solar Cells: Theory, Experiment, and Device Simulation by Wolfgang Tress pages 34-36

[16] Sinton RA, Swanson RM. Recombination in highly injected silicon. Electron Devices, IEEE Transactions on. 1987; 34:1380-1389.

[17] Altermatt PP, Sinton RA, Heiser G. Improvements in numerical modelling of highly injected crystalline silicon solar cells. Solar Energy Materials and Solar Cells [Internet]. 2001; 65:149-155(7).

[18] *Ultrafast Dynamical Processes in Semiconductors*. edited by Kong-Thon Tsen. Springer Science & Business Media, 2004. page 267

[19] F. Stern, *J. appl. Phys.* **47**, 5382 (1976).

[20] H. C. Casey Jr and F. Stern, *J. appl. Phys.* **47**, 631 (1976).

[21] Goetzberger, Adolf et.al. *Crystalline Silicon Solar Cells*. Chichester: John Wiley & Sons Ltd., 1998.

[22] R.M. Briggs, G.M. Miller and H.A. Atwater, "Modifying the radiative quantum efficiency of erbium-doped glass in silicon slot waveguides", *6th IEEE International Conference on Group IV Photonics*, pp. 223-225, 2009.

[23] Bragg, W.H.; Bragg, W.L. (1913). "The Reflexion of X-rays by Crystals". Proc R. Soc. Lond. A. **88** (605): 428–38.

[24] J. Cernogora, “Photoluminescence in a-C:H.” phys. Stat. sol. (b) **2**01, 303 (1997)

[25] Rusli, Gehan A. J. Amaratunga, and S. R. P. Silva, Thin Solid Films 270, 160 (1995).

[26] Rusli, J. Robertson, and G. A. J. Amaratunga, J. Appl. Phys. **80**, 2998 (1996).

[27] E. Billa, E. Koutsoula, E.G. Koukios, “Fluorescence analysis of paper pulps,” Bioresource Technology, vol. 67, pp. 25–33, 1999.

[28] A. Savitzky and M. J. E. Golay, “Soothing and differentiation of data by simplified least squares procedures,” Anal. Chem., vol. 36, pp. 1627–1639, 1964.

[39] A. Kostyukov, “Photoluminescence of Cr3+ in nanostructured Al2O3 synthesized by evaporation using a continuous wave CO2 laser,” RSC Adv., 2016, **6**, 2072

[30] D. Lapraz, P. Iacconi, D. Daviller, and B. Guilhot, Phys. Stat. Sol. (a) **126**, 521 (1991).

[31] Maiman, T.H. (1960) “Stimulated Optical Radiation in Ruby”. Nature, **187** 4736, pp. 493-494.

[32] H. D. Chen “Carbon incorporation during growth of GaAs by TEGa-AsH_3 base low-pressure metalorganic chemical vapor deposition” J. Appl. Phys. **73**, 7851 (1993);

[33] H. D. Chen “Photoluminescence of Heavily p-Type-Doped GaAs: Temperature and Concentration Dependences” J. Appl. Phys. **33**, 1920 (1994);

[34] Lei Wang, Nancy M. Haegel, and Jeremiah R. Lowney “Band-to-band photoluminescence and luminescence excitation in extremely heavily carbon-doped epitaxial GaAs” Phys. Rev. B **49**, 10976 (1994)

[35] G. Borghs, K. Bhattacharyya, K. Deneffe, P. Van Mieghem and R. Mertens “Band-gap narrowing in highly doped n- and p-type GaAs studied by photoluminescence spectroscopy” J. Appl. Phys. **66**, 4381 (1989);

[36] C. J. Hwang, “Calculation of Fermi Energy and Bandtail Parameters in Heavily Doped and Degenerate *n*-Type GaAs” J. Appl. Phys. **41**, 2668 (1970);

[37] Nam-Young Lee, Kyu-Jang Lee, Chul Lee, Jae-Eun Kim, Hae Yong Park, Dong-Hwa Kwak, Hee-Chul Lee and H. Lim, “Determination of conduction band tail and Fermi energy of heavily Si-doped GaAs by room-temperature photoluminescence” J. Appl. Phys. **78**, 3367 (1995);

[38] R. A. Street. Hydrogenated Amorphous Silicon. Cambridge University Press, Cambridge, 1991.

[39] D. Weaire and M. F. ThorpePhys. Rev. B 4, 2508 – Published 15 October 1971

[40] M. F. Thorpe and D. Weaire Phys. Rev. B 4, 3518 – Published 15 November 1971

[41] Journal of Applied Physics 118(11):115502 · September 2015

[42] W. Futako “The structure of 1.5–2.0 eV band gap amorphous silicon films prepared by chemical annealing” Journal of Non-Crystalline Solids **266-269**, 630 (2000)

[43] Bouchacourt M and Thevenot F 1985 J. Mater. Sci. **20** 1237–47

[44] Simeone, D.; Mallet, C.; Dubuisson, P.; Baldinozzi, G.; Gervais, C.; Maquet, J. J. Nucl. Mater. 2000, **277**, 1

[45] Dowben P A 1995 USPTO 5,468, 978

[46] Hwang S-D, Yang K, Dowben P A, Ahmad A A, Ianno N J, Li J Z, Lin J Y, Jiang H X and McIlroy D N 1997 Appl. Phys. Lett. **70** 1028–30

[47] Robertson B W, Adenwalla S, Harken A, Welsch P, Brand J I, Dowben P A and Claassen J P 2002 Appl. Phys. Lett. **80** 3644–6

[48] Schutte, W.J.; De Boer, J.L.; Jellinek, F. (1986). "Crystal Structures of Tungsten Disulfide and Diselenide". Journal of Solid State Chemistry **70**: 207–209

[49] A. Pospischil, M. M. Furchi, T. Mueller, “Solar-energy conversion and light emission in an atomic monolayer p–n diode” *Nature Nanotechnology* **9**, 257–261 (2014)

[50] A. Arora, et al. “Excitonic resonances in thin films of WSe2: from monolayer to bulk material.” Nanoscale, 2015, **7**, 10421-10429

[51] Tonndorf, Philipp, et al. "Photoluminescence emission and Raman response of monolayer MoS 2, MoSe 2, and WSe 2." *Optics express* 21.4 (2013): 4908-4916.

[52] Britt J., Ferekides C., Thin film CdS/CdTe solar cell with 15.8% efficiency, Appl. Phys. Lett. 1993 (62) 2851-2852.

[53] Ferekides C. S., Marinskiy D., Viswanathan V., Tetali B., Palekis V., Selvaraj P., Morel D. L. High efficiency CSS CdTe solar cells, Thin Solid Films, 2000 (361-362) 520-526.

[54] M. Marwede and A. Reller (2012). "Future recycling flows of tellurium from cadmium telluride photovoltaic waste". *Resources, Conservation and Recycling.* **69**: 35–49.

[55] Ma, Qinglei, “Growth, Characterization and Simulation of Tungsten Selenide Thin Films for Photovoltaic Applications” (2016). *Theses and Dissertations from Electrical & Computer Engineering.* Paper 69.

[56] Chen, Gang et al. *Bis-BN Cyclohexane: A Remarkably Kinetically Stable Chemical Hydrogen Storage Material*. J. Am. Chem. Soc. 2015, 137, 134−137

[57] Goetzberger, Adolf et.al. *Crystalline Silicon Solar Cells*. Chichester: John Wiley & Sons Ltd., 1998.

[58] Z. Ren, Private Correspondence (2016)

[59] M. S. Dresselhaus, "Solid State Physics Part II Optical Properties of Solids", vol. 6, 2001.

[60] Y. S. Tsuo, E. B. Smith and S. K. Deb, "Ion beam hydrogenation of amorphous silicon", Appl. Phys. Lett. **51**, 1436 (1987)